Supplemental Material to: Nonreciprocity as a generic route to traveling states

Zhihong You,[1,*] Aparna Baskaran,[2] and M. Cristina Marchetti[1,†]

[1] *Department of Physics, University of California Santa Barbara, Santa Barbara, CA 93106, USA*
[2] *Martin Fisher school of Physics, Brandeis University, Waltham, MA 02453, USA*

I. ONE-MODE APPROXIMATION

In this section, we show the derivation of Eq. (3) and Eq. (4) in the main text using the Fourier-Galerkin method [1].

A. General form of mode equations

Let us start from the 1D version of Eq. (1),

$$\frac{\partial \phi_A}{\partial t} = \partial_x \left[\left(\chi_A + \phi_A^2 - \gamma_A \partial_x^2 \right) \partial_x \phi_A \right] + \kappa_{AB} \partial_x^2 \phi_B, \tag{S1a}$$

$$\frac{\partial \phi_B}{\partial t} = \partial_x \left(\chi_B \partial_x \phi_B \right) + \kappa_{BA} \partial_x^2 \phi_A. \tag{S1b}$$

Here, we've ignored $\phi_B^2 - \gamma_B \partial_x^2$ as in the main text. To apply the Fourier-Galerkin method, we express ϕ_μ as a superposition of Fourier modes:

$$\phi_\mu(x,t) = \sum_{j=-\infty}^{\infty} \hat{\phi}_\mu^j(t) e^{i q_j x}, \tag{S2}$$

where the wave number $q_j = 2\pi j/L$, and

$$\hat{\phi}_\mu^j(t) = \frac{1}{L} \int_0^L \phi_\mu(x,t) e^{-i q_j x} dx, \tag{S3}$$

are the complex amplitudes of the Fourier modes. The dynamical equations for the Fourier modes obtained from Eq. S1 then are [1]:

$$\frac{d\hat{\phi}_A^j(t)}{dt} = -q_j^2 \left[\left(\chi_A + \gamma_A q_j^2 \right) \hat{\phi}_A^j + \kappa_{AB} \hat{\phi}_B^j \right] - \sum_{j_1, j_2} \left(q_{j_1}^2 + 2 q_{j_1} q_{j_2} \right) \hat{\phi}_A^{j_1} \hat{\phi}_A^{j_2} \hat{\phi}_A^{j - j_1 - j_2}, \tag{S4a}$$

$$\frac{d\hat{\phi}_B^j(t)}{dt} = -q_j^2 \left(\chi_B \hat{\phi}_B^j + \kappa_{BA} \hat{\phi}_A^j \right). \tag{S4b}$$

By solving for the mode amplitudes $\hat{\phi}_\mu^j(t)$ and transforming the results back to physical space with Eq. (S2), one can obtain the dynamics of $\phi_\mu(x,t)$. This method is usually referred to as the spectral method [1]. For the particular system at hand, numerical solutions of the full theory show that the first mode is dominant in determining the dynamical steady states discussed in the main text (Fig. S1). This is our motivation for considering a reduced theory for our system by truncating the Fourier-Galerkin representation at the level of the first mode.

B. One-mode approximation

Since ϕ_A and ϕ_B are conserved quantities, both $\hat{\phi}_A^0$ and $\hat{\phi}_B^0$ are time independent. Setting $\hat{\phi}_\mu^j = 0$ for $|j| > 1$, and $q_j = j$, Eq. S4a reduces to

$$\frac{d\hat{\phi}_A^1(t)}{dt} = -\left(\alpha_A + |\hat{\phi}_A^1|^2 \right) \hat{\phi}_A^1 - (\kappa - \delta) \hat{\phi}_B^1, \tag{S5}$$

* Corresponding author: youz@ucsb.edu
† Corresponding author: cmarchetti@ucsb.edu

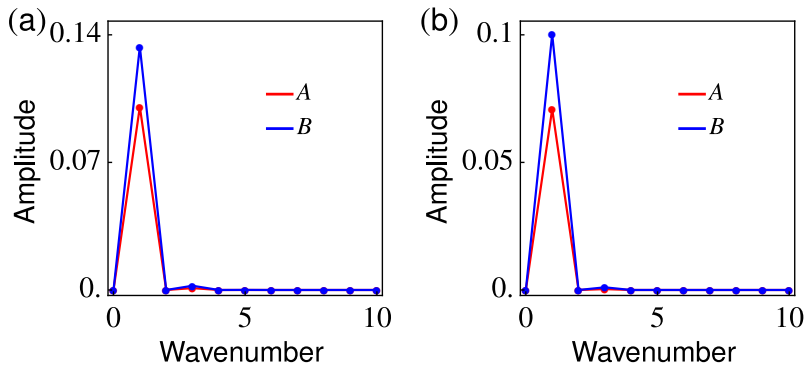

Fig. S1. Amplitudes of Fourier modes $|\hat{\phi}^j_\mu|$ at the steady (a) static and (b) traveling states. We used $\chi_A = -0.05$ and (a) $\delta = \kappa$ and (b) $\delta = 3\kappa$.

where $\alpha_A = \chi_A + \gamma_A + (\phi^0_A)^2$. Similarly, for $\hat{\phi}^1_B$, we have

$$\frac{d\hat{\phi}^1_B(t)}{dt} = -\alpha_B \hat{\phi}^1_B - (\kappa + \delta)\hat{\phi}^1_A, \tag{S6}$$

where $\alpha_B = \chi_B$. These are Eq. (3) in the main text and constitute the one mode approximation for our full theory.

Expressing the complex quantities $\hat{\phi}^1_\mu$ in terms of their amplitude and phase, $\hat{\phi}^1_\mu = \rho_\mu e^{i\theta_\mu}$, Eqs. (S5) and (S6) can be recast as

$$\frac{d\rho_A}{dt} = -(\alpha_A + \rho_A^2)\rho_A - (\kappa - \delta)\rho_B \cos\theta, \tag{S7a}$$
$$\frac{d\rho_B}{dt} = -\alpha_B \rho_B - (\kappa + \delta)\rho_A \cos\theta, \tag{S7b}$$
$$\frac{d\theta}{dt} = \left[(\kappa - \delta)\rho_A^{-1}\rho_B + (\kappa + \delta)\rho_A \rho_B^{-1}\right]\sin\theta, \tag{S7c}$$
$$\frac{d\Phi}{dt} = \left[(\kappa - \delta)\rho_A^{-1}\rho_B - (\kappa + \delta)\rho_A \rho_B^{-1}\right]\sin\theta, \tag{S7d}$$

with $\Phi = \theta_A + \theta_B$ and $\theta = \theta_A - \theta_B$. These are Eq. (4) in the main text.

II. STEADY STATES AND THEIR STABILITY

In this section, we identify the steady states in the one-mode approximation, and study their stability.

a. Steady states. The steady states are obtained as the fixed points of Eqs. (S7a)-(S7c). Note that Φ is slaved by the other three quantities. The solution $\rho_A = 0$ and $\rho_B = 0$ corresponds to the homogeneous state, and is referred to as the trivial fixed point F_H in the main text. In this case, the phases are not well defined.

A second fixed point is obtained when $\sin\theta = 0$ or $\theta = 0, \pi$. Since Eq. (S7b) yields $\rho_B = -\alpha_B^{-1}(\kappa + \delta)\rho_A \cos\theta$ and the amplitudes ρ_μ must be positive the only acceptable solution is $\theta = \pi$. The second fixed point, F_S, is then given by

$$\rho^s_A = \left[(\kappa^2 - \delta^2)/\alpha_B - \alpha_A\right]^{1/2}, \tag{S8a}$$
$$\rho^s_B = (\kappa + \delta)\rho^s_A/\alpha_B, \tag{S8b}$$
$$\theta^s = \pi, \tag{S8c}$$

In order for F_S to exist as a physical state of the system, the argument of the square root in Eq. (S8a) must be real, which requires $\kappa^2 - \delta^2 > \alpha_B \alpha_A$, as given in the main text.

Finally, when $\sin\theta \neq 0$ one can have a third solution F_T with $\dot{\Phi}$ finite, corresponding to spatial modulations that

travel at the fixed velocity $v = \dot{\Phi}/2$. This requires $\left[(\kappa-\delta)\rho_A^{-1}\rho_B + (\kappa+\delta)\rho_A\rho_B^{-1}\right] = 0$ and it is given by

$$\rho_A^t = (-\alpha_A - \alpha_B)^{1/2}, \tag{S9a}$$
$$\rho_B^t = \sqrt{(\delta+\kappa)/(\delta-\kappa)}\ \rho_A^t, \tag{S9b}$$
$$\theta^t = \arccos\left(-\sqrt{\frac{\alpha_B^2}{\delta^2-\kappa^2}}\right). \tag{S9c}$$

The requirement that the arguments of all square roots be positive and the argument of $\arccos(\cdot)$ have an absolute value no larger than 1 yields the conditions of existence for F_T as

$$\alpha_A < -\alpha_B, \tag{S10a}$$
$$\delta^2 - \kappa^2 \geq \alpha_B^2. \tag{S10b}$$

As we will see below, the first one describes the instability of the stationary spatial modulation F_S, while the second one demands that nonreciprocity to be strong enough for the traveling pattern to appear.

b. Linear stability. Now we examine the stability of the fixed points, which is controlled by the eigenvalues of the Jacobian matrix evaluated at the fixed points:

$$\mathbf{M} \equiv \begin{bmatrix} \frac{\partial\dot{\rho}_A}{\partial\rho_A} & \frac{\partial\dot{\rho}_A}{\partial\rho_B} & \frac{\partial\dot{\rho}_A}{\partial\theta} \\ \frac{\partial\dot{\rho}_B}{\partial\rho_A} & \frac{\partial\dot{\rho}_B}{\partial\rho_B} & \frac{\partial\dot{\rho}_B}{\partial\theta} \\ \frac{\partial\dot{\theta}}{\partial\rho_A} & \frac{\partial\dot{\theta}}{\partial\rho_B} & \frac{\partial\dot{\theta}}{\partial\theta} \end{bmatrix} = \begin{bmatrix} -\alpha_A - 3\rho_A^2 & -(\kappa-\delta)\cos\theta & (\kappa-\delta)\rho_B\sin\theta \\ -(\kappa+\delta)\cos\theta & -\alpha_B & (\kappa+\delta)\rho_A\sin\theta \\ \left(\frac{\kappa+\delta}{\rho_B} - \frac{(\kappa-\delta)\rho_B}{\rho_A^2}\right)\sin\theta & \left(\frac{\kappa-\delta}{\rho_A} - \frac{(\kappa+\delta)\rho_A}{\rho_B^2}\right)\sin\theta & \left(\frac{(\kappa-\delta)\rho_B}{\rho_A} + \frac{(\kappa+\delta)\rho_A}{\rho_B}\right)\cos\theta \end{bmatrix}. \tag{S11}$$

With our convention, an instability corresponds to a positive real part of the largest eigenvalue.

At the trivial fixed point, F_H, the phases are undetermined and one can simply examine the stability of Eqs. (S5) and (S6). The corresponding Jacobian matrix at F_H is

$$\mathbf{M}_H = \begin{bmatrix} -\alpha_A & -\kappa_{AB} \\ -\kappa_{BA} & -\alpha_B \end{bmatrix}, \tag{S12}$$

with eigenvalues

$$\lambda_\pm^h = \frac{1}{2}\left[-(\alpha_A+\alpha_B) \pm \sqrt{(\alpha_A-\alpha_B)^2 + 4(\kappa^2-\delta^2)}\right]. \tag{S13}$$

As discussed in the main text, the trivial fixed point F_H can become unstable through different routes, depending on the sign of the argument of the square root in Eq. (S13). When $(\alpha_A-\alpha_B)^2 + 4(\kappa^2-\delta^2) > 0$, $\lambda_\pm^h$ are real (Fig. S2),

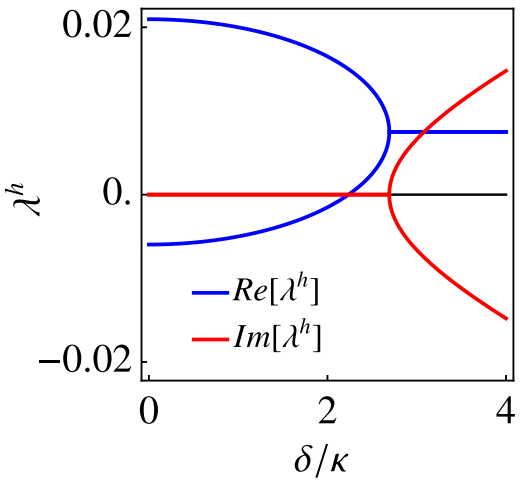

Fig. S2. Real (blue lines) and imaginary (red lines) parts of eigenvalues $\lambda_\pm^h$ as functions of δ for $\chi_A = -0.06$ showing the change from diffusive to propagating modes. An instability is signaled by $Re[\lambda] > 0$.

and the homogeneous state becomes unstable via a diffusive instability when λ_+^h becomes positive for $\kappa^2-\delta^2 > \alpha_A\alpha_B$. On the other hand, if $(\alpha_A-\alpha_B)^2+4(\kappa^2-\delta^2)<0$, $\lambda_\pm^h$ are complex conjugate (Fig. S2), and the system becomes unstable via an oscillatory instability when $Re[\lambda_\pm^h]$ becomes positive for $\alpha_A < -\alpha_B$.

To investigate the stability of F_S, we evaluate the Jacobian matrix given in Eq. (S11) at the fixed point, with the result

$$\mathbf{M}_S = \begin{bmatrix} 2\alpha_A - 3\frac{\kappa^2-\delta^2}{\alpha_B} & \kappa-\delta & 0 \\ \kappa+\delta & -\alpha_B & 0 \\ 0 & 0 & -\alpha_B - \frac{\kappa^2-\delta^2}{\alpha_B} \end{bmatrix} \tag{S14}$$

Fluctuations in ρ_A and ρ_B are coupled. Their relaxation is controlled by the eigenvalues

$$\lambda_\pm^s = \frac{1}{2}\left[2\alpha_A-\alpha_B-3\frac{\kappa^2-\delta^2}{\alpha_B}\right] \pm \frac{1}{2}\sqrt{\left[2\alpha_A+\alpha_B-3\frac{\kappa^2-\delta^2}{\alpha_B}\right]^2+4(\kappa^2-\delta^2)} \tag{S15}$$

which always have a negative real part in the region of parameters where F_S exists, hence are stable. On the other hand, fluctuations in the relative phase θ are controlled by

$$\lambda_\theta^s = -\frac{\delta_c^2-\delta^2}{\alpha_B}\,, \tag{S16}$$

where $\delta_c = \sqrt{\kappa^2+\alpha_B^2}$. The eigenvalue is real and positive for $\delta > \delta_c$, signaling the growth of phase fluctuations that destabilize the stationary demixed state, giving rise to traveling patterns. Finally, the eigenvalues of $\mathbf{M}$ at F_T are too complicated to be instructive. It can, however, be demonstrated numerically, that they are always negative, so the traveling patterns corresponding to this fixed point are always stable, in the region of parameters where it exists.

III. CRITICAL POINT AS AN EXCEPTIONAL POINT

As mentioned in the main text, the drift bifurcation induced by the nonreciprocal interspecies interaction belongs to a generic class of phase transitions which has been studied in optical and quantum systems [2–4], and more recently in nonreciprocally interacting polar active fluids [5]. This type of phase transitions is known to occur at a so-called exceptional point that separates a PT-symmetric phase from a phase with broken PT symmetry [3, 5].

To clarify these concepts, let us return to the compact form of our one-mode model written in terms of complex Fourier amplitudes, as given in Eq. (3) of the main text,

$$\frac{d}{dt}\begin{bmatrix}\hat\phi_A \\ \hat\phi_B\end{bmatrix} = \begin{bmatrix} -\alpha_A - |\hat\phi_A|^2 & -(\kappa-\delta) \\ -(\kappa+\delta) & -\alpha_B \end{bmatrix}\begin{bmatrix}\hat\phi_A \\ \hat\phi_B\end{bmatrix} \equiv \mathbf{D}[\hat\phi_A]\begin{bmatrix}\hat\phi_A \\ \hat\phi_B\end{bmatrix}\,, \tag{S17}$$

where we have dropped the mode superscript 1 to simplify the notation. The 2×2 non-Hermitian matrix $\mathbf{D}[\hat\phi_A]$ in Eq. (S17) controls the system's dynamics. The stationary fixed point F_S is obtained by solving $\mathbf{D}[\hat\phi_A]=0$ and it is given by

$$\mathbf{u}^s \equiv \begin{bmatrix}\hat\phi_A^s \\ \hat\phi_B^s\end{bmatrix} = \begin{bmatrix} \sqrt{(\kappa^2-\delta^2)/\alpha_B - \alpha_A}\; e^{i\theta_0} \\ -\alpha_B^{-1}(\kappa+\delta)\hat\phi_A^s \end{bmatrix}, \tag{S18}$$

where θ_0 is an undetermined phase indicating translation of ϕ_μ in space. Since $\hat\phi_B^s \sim -\hat\phi_A^s$, the two complex fields are out of phase and this fixed point corresponds exactly to the out-of-phase static patterns described in the main text.

Let us now assume that there exists a stationary nontrivial solution that solves $\mathbf{D}[\hat\phi_A^0]\begin{bmatrix}\hat\phi_A^0 \\ \hat\phi_B^0\end{bmatrix} = 0$ and evaluate eigenvalues and eigenvectors of $\mathbf{D}_0 \equiv \mathbf{D}[\hat\phi_A^0]$ and then examine their behavior at the stationary fixed point given in (S18). These are given by

$$\lambda_\pm = -\frac{1}{2}\left(\alpha_B+\alpha_A+|\hat\phi_A^0|^2\right) \pm \frac{1}{2}\sqrt{\Delta}\,, \tag{S19}$$

where $\Delta = \left(\alpha_B-\alpha_A-|\hat\phi_A^0|^2\right)^2 + 4(\kappa^2-\delta^2)$ and

$$\mathbf{u}_\pm = C_\pm\begin{bmatrix}-(\lambda_\pm+\alpha_B) \\ \kappa+\delta\end{bmatrix} \tag{S20}$$

where $C_\pm$ are normalization constants. If $\Delta > 0$, the eigenvalues are real. If stable, the solutions will be stationary in this regime. Note the matrix $\mathbf{D}_0$ is in general different form the linear matrix that controls the stability of fixed points. If $\Delta < 0$, the eigenvalues are complex conjugate, signaling the onset of an oscillatory solutions. The point $\Delta = 0$ corresponds to $\delta^2 = \kappa^2 + (\alpha_B - \alpha_A - |\hat{\phi}_A^0|^2)^2/4$. Substituting $\phi_A^0 = \phi_A^s$, we find that the modes change from real to complex conjugates at $\delta = \delta_c = \sqrt{\kappa^2 + \alpha_B^2}$. At this point, solutions change from stationary to oscillatory.

We also note that when evaluated at the fixed point F_S the eigenvalues become

$$\lambda_\pm = -\frac{1}{2\alpha_B}\left((\delta_c^2 - \delta^2) \pm |\delta_c^2 - \delta^2|\right) \ , \tag{S21}$$

or

$$\lambda_1^s = 0 \ , \tag{S22}$$

$$\lambda_2^s = -\frac{\delta_c^2 - \delta^2}{\alpha_B} \tag{S23}$$

At the critical point $\delta = \delta_c$, the two eigenvalues are equal and the eigenvectors become co-linear. In addition, the solutions change from stationary to oscillatory. This is what is referred to as an exceptional point [6]. This behavior is also associated with the fact that the matrix $\mathbf{D}[\hat{\phi}_A]$ evaluated at the steady state (S18) is given by

$$\mathbf{D}_s \equiv \mathbf{D}[\hat{\phi}_A^s] = \begin{bmatrix} -(\kappa^2 - \delta^2)/\alpha_B & -(\kappa - \delta) \\ -(\kappa + \delta) & -\alpha_B \end{bmatrix} \tag{S24}$$

hence $\det[\mathbf{D}_s] = 0$.

More precisely, to elucidate the nature of the drift instability as an exceptional point, we examine the matrix that controls the linear stability of the stationary density modulated state F_S. We show below that the instability occurs when one of the eigenmodes of such a matrix coalesces with the Goldstone mode associated with spontaneously broken translational symmetry of the modulated state [4, 5]. To demonstrate this, we linearize (S17) about the static fixed point F_S to obtain coupled equations for the complex fluctuations $\delta\hat{\phi}_\mu$ of the phase fields, given by

$$\frac{d\delta\mathbf{u}}{dt} = \mathbf{L} \cdot \delta\mathbf{u}, \tag{S25}$$

where

$$\delta\mathbf{u} = \begin{pmatrix} \delta\hat{\phi}_A \\ \delta\hat{\phi}_B \\ \delta\hat{\phi}_A^* \\ \delta\hat{\phi}_B^* \end{pmatrix} \tag{S26}$$

and

$$\mathbf{L} = \begin{pmatrix} -\alpha_A - 2|\hat{\phi}_A^s|^2 & -(\kappa - \delta) & -(\hat{\phi}_A^s)^2 & 0 \\ -(\kappa + \delta) & -\alpha_B & 0 & 0 \\ -(\hat{\phi}_A^{s*})^2 & 0 & -\alpha_A - 2|\hat{\phi}_A^s|^2 & -(\kappa - \delta) \\ 0 & 0 & -(\kappa + \delta) & -\alpha_B \end{pmatrix} \tag{S27}$$

is the matrix controlling the linear stability of the fixed point. We note that Eqs. (S17) are invariant under an arbitrary global translation $\hat{\phi}_\mu \to \hat{\phi}_\mu e^{i\delta\theta}$. The breaking of translational symmetry associated with the emergence of the spatially-modulated de-mixed stationary state from the homogeneous state is accompanied by the appearance of a zero mode associated with fluctuations in the total phase of the complex field amplitudes which is the Goldstone mode of the transition. The second PT-breaking transition to the traveling state occurs when another eigenmode of $\mathbf{L}$ coalesces with the Goldstone mode at the exceptional point.

The linear matrix $\mathbf{L}$ has four eigenvalues

$$\lambda_1^\pm = \frac{1}{2}\left[-\alpha_B - (\kappa^2 - \delta^2)/\alpha_B \pm \sqrt{\Delta_1}\right] \tag{S28a}$$

$$\lambda_2^\pm = \frac{1}{2}\left[-\alpha_B + 2\alpha_A - 3(\kappa^2 - \delta^2)/\alpha_B \pm \sqrt{\Delta_2}\right] \tag{S28b}$$

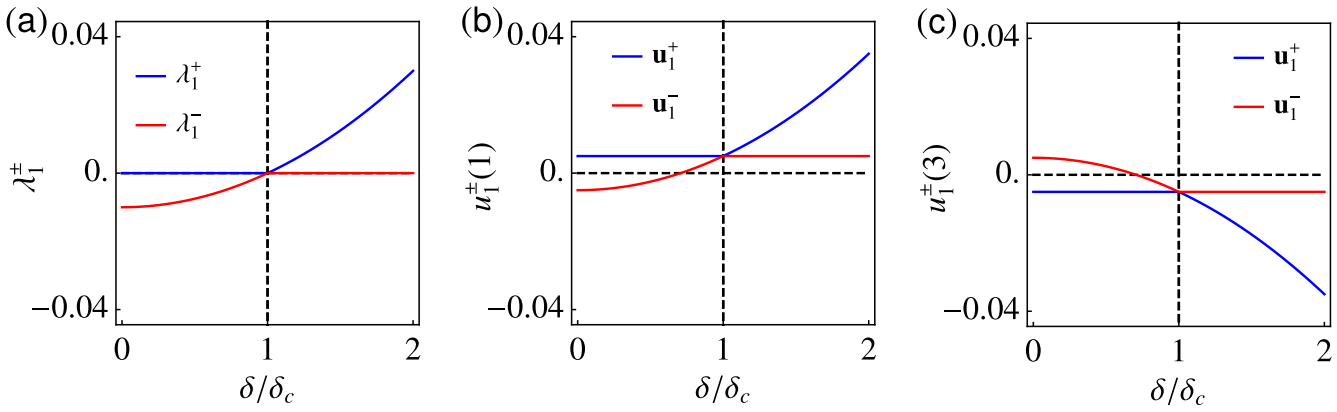

Fig. S3. (a) Eigenvalues and the (b) first and (c) third elements of eigenvectors of the matrix $\mathbf{L}$ evaluated at the static modulated state F_S. The blue lines corresponds to the Goldstone mode $\mathbf{u}_1^+$, while the red line shows the mode $\mathbf{u}_1^-$, which coalesces with the Goldstone mode at $\delta = \delta_c$.

with the corresponding eigenmodes

$$\mathbf{u}_1^\pm = \begin{pmatrix} \frac{1}{2}\left[\alpha_B - (\kappa^2-\delta^2)/\alpha_B \pm \sqrt{\Delta_1}\right] \\ -(\kappa+\delta) \\ -\frac{1}{2}\left[\alpha_B - (\kappa^2-\delta^2)/\alpha_B \pm \sqrt{\Delta_1}\right] \\ (\kappa+\delta) \end{pmatrix}, \quad \mathbf{u}_2^\pm = \begin{pmatrix} -\frac{1}{2}\left[\alpha_B + 2\alpha_A - 3(\kappa^2-\delta^2)/\alpha_B \pm \sqrt{\Delta_2}\right] \\ (\kappa+\delta) \\ -\frac{1}{2}\left[\alpha_B + 2\alpha_A - 3(\kappa^2-\delta^2)/\alpha_B \pm \sqrt{\Delta_2}\right] \\ (\kappa+\delta) \end{pmatrix}, \tag{S29}$$

where

$$\Delta_1 = \left[\alpha_B + (\kappa^2-\delta^2)/\alpha_B\right]^2 \tag{S30a}$$

$$\Delta_2 = \left[\alpha_B + 2\alpha_A - 3(\kappa^2-\delta^2)/\alpha_B\right]^2 + 4\left(\kappa^2-\delta^2\right) \tag{S30b}$$

For $\delta < \delta_c$, $\lambda_1^+ = 0$ (blue line in Fig. S3a), hence $\mathbf{u}_1^+$ corresponds to the Goldstone mode arising from the spontaneous breaking of translational symmetry. At $\delta = \delta_c$, $\Delta_1 = 0$ and λ_1^- vanishes and $\mathbf{u}_1^-$ becomes colinear with the eigenvector $\mathbf{u}_1^+$ of the Goldstone mode (Fig. S3b–S3c), giving rise to the PT breaking transition or drift bifurcation, which corresponds to an exceptional point [4, 5].

IV. TWO-DIMENSIONAL CASE

We show here that a static-to-traveling transition driven by nonreciprocal interactions also occurs in two dimensional systems, albeit with a richer dynamics. The detailed analysis is left for future work. The goal of this section is to highlight that the qualitatve behavior remains the same. We have integrated numerically Eq. (1) from the main text in a two-dimensional periodic box of size $L \times L$, with $L = 2\pi$ and the same parameter values as in the main text: $\chi_A = -0.05$, $\chi_B = 0.005$, $\gamma_A = 0.04$, $\gamma_B = 0$, $\kappa = 0.005$, $\phi_A^0 = \phi_B^0 = 0$. We have then examined the effect of nonreciprocity by increasing δ.

As in one dimension, we observe a transition from static to traveling modulations with increasing nonreciprocity, as shown in Figs. S4a–S4d and Movie S1-S2. The orientation of the band is determined by random fluctuations and by the initial concentration. The expression for drift velocity obtained in one dimension, $v = \pm\sqrt{\delta^2 - \delta_c^2}$, with $\delta_c = \sqrt{\kappa^2 + \alpha_B^2}$, gives an excellent parameter-free fit to the velocity of the traveling pattern in 2D, as shown in Fig. S4g. In addition to traveling modulations of the fields, in 2D we also observe oscillatory patterns that are absent in the 1D system. This consists of high/low concentration region of each species that periodically split and merge (Figs. S4e–S4f and and Movie S3). The oscillatory state also originates from the nonreciprocal interactions, as evidenced by the fact that it only appears when $\delta > \delta_c$, and the oscillating frequency increases with nonreciprocity (Fig. S4h). In the parameter region we have explored, the traveling and oscillatory states are both stable, and the state is selected by the initial condition.

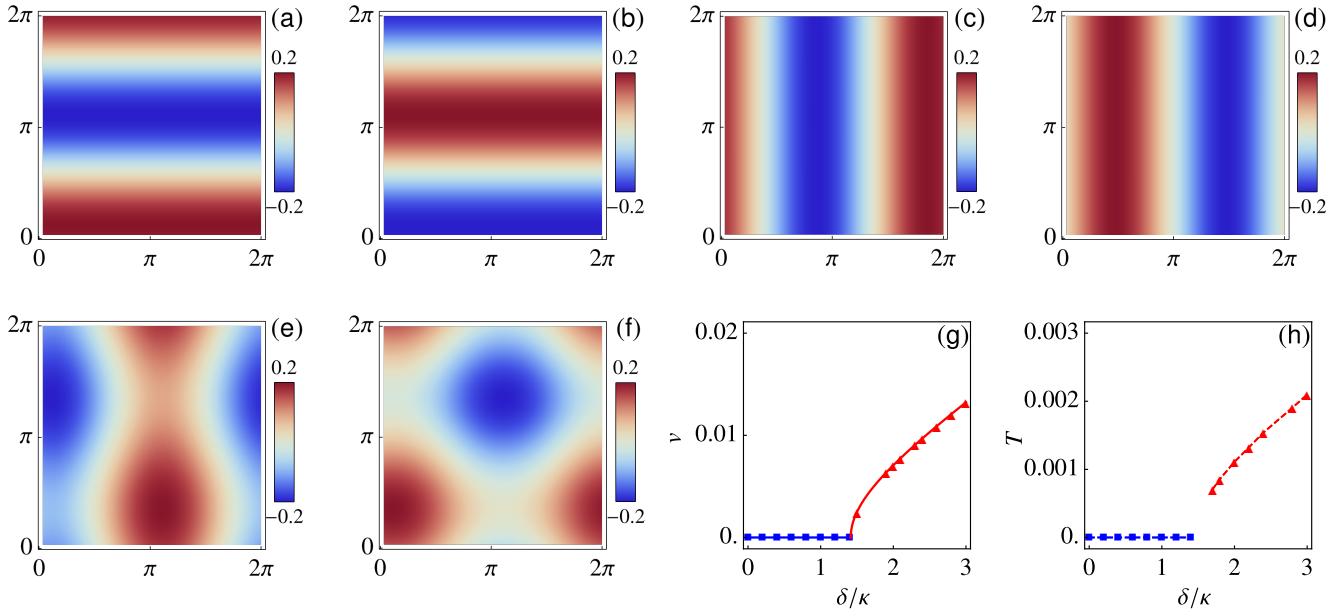

Fig. S4. Pattern formations in two-dimensional systems at the (a–b) static, (c–d) traveling, and (e–f) oscillatory states. Panels (a,c,e) show ϕ_A, while (b,d,f) ϕ_B, highlighting the phase relation of the two fields. In the stationary demixed state (a–b, $\delta = \kappa$), ϕ_A and ϕ_B are out-of-phase, while in the traveling state (c–d, $\delta = 3\kappa$) ϕ_A and ϕ_B have a constant phase shift different from π, and the pattern is traveling from left to right. In the oscillatory state(e–f, $\delta = 3\kappa$), the high concentration regions of both ϕ_A and ϕ_B periodically split and merge. Panels (g) and (h) shows the travellng speed and oscillating frequency of the traveling and oscillatory patterns, respectively. Both increases monotonically with the nonreciprocity δ. In panel (g), the solid line corresponds to $v = \sqrt{\delta^2 - \delta_c^2}$, with $\delta_c = \sqrt{\kappa^2 + \alpha_B^2}$.

V. BI-SUPERCRITICAL SYSTEMS

In the main text, we have considered the case when field A is supercritical, but field B is subcritical and its dynamics is purely relaxational. To demonstrate the generality of our findings, we have also considered the case where both fields are supercritical, as obtained when $\chi_A < 0$ and $\chi_B < 0$. In this case, restoring the term $\phi_B^2 - \gamma_B \partial_x^2$, the equations become

$$\frac{\partial \phi_A}{\partial t} = \partial_x \left[\left(\chi_A + \phi_A^2 - \gamma_A \partial_x^2 \right) \partial_x \phi_A \right] + \kappa_{AB} \partial_x^2 \phi_B, \tag{S31a}$$

$$\frac{\partial \phi_B}{\partial t} = \partial_x \left[\left(\chi_B + \phi_B^2 - \gamma_B \partial_x^2 \right) \partial_x \phi_B \right] + \kappa_{BA} \partial_x^2 \phi_A. \tag{S31b}$$

Numerical integration of Eq. (S31) yields again stationary demixed states that transition to traveling ones with increasing nonreciprocity, as shown in Fig. S5.

Following the procedure described above, we can obtain the one-mode approximation for Eq. (S31) as

$$\frac{d\hat{\phi}_A^1(t)}{dt} = -\left(\alpha_A + |\hat{\phi}_A^1|^2 \right) \hat{\phi}_A^1 - (\kappa - \delta) \hat{\phi}_B^1, \tag{S32a}$$

$$\frac{d\hat{\phi}_B^1(t)}{dt} = -\left(\alpha_B + |\hat{\phi}_B^1|^2 \right) \hat{\phi}_B^1 - (\kappa + \delta) \hat{\phi}_A^1, \tag{S32b}$$

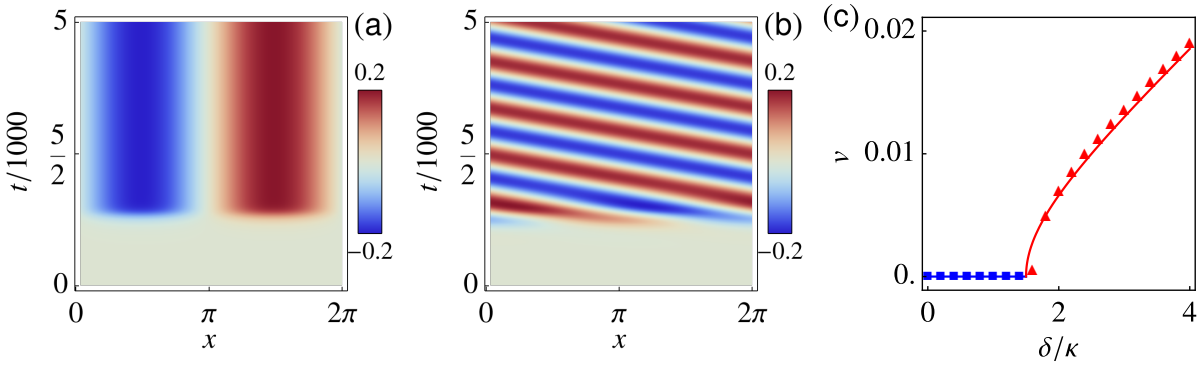

Fig. S5. Drift instability in bi-supercritical systems. (a–b) Spatiotemporal patterns of ϕ_A in (a) static ($\delta = \kappa$) and (b) traveling states ($\delta = 2\kappa$). (c) Speed of the traveling modulation as a function of nonreciprocity δ/κ. The red line is a fit to the mean-field theory with $v = \sqrt{\delta^2 - \delta_c^2}$, where $\delta_c = 1.5\kappa$ is extracted from the best fit to the data. All results shown are for $\chi_A = \chi_B = -0.05$, $\gamma_A = \gamma_B = 0.04$, $\kappa = 0.005$, and $L = 2\pi$.

where $\alpha_\mu = \chi_\mu + \gamma_\mu + (\phi_\mu^0)^2$. In the amplitude-phase space, Eq. S32 can be rewritten as

$$\frac{d\rho_A}{dt} = -(\alpha_A + \rho_A^2)\rho_A - (\kappa - \delta)\rho_B \cos\theta, \tag{S33a}$$

$$\frac{d\rho_B}{dt} = -(\alpha_B + \rho_B^2)\rho_B - (\kappa + \delta)\rho_A \cos\theta, \tag{S33b}$$

$$\frac{d\theta}{dt} = \left[(\kappa - \delta)\rho_A^{-1}\rho_B + (\kappa + \delta)\rho_A\rho_B^{-1}\right]\sin\theta, \tag{S33c}$$

$$\frac{d\Phi}{dt} = \left[(\kappa - \delta)\rho_A^{-1}\rho_B - (\kappa + \delta)\rho_A\rho_B^{-1}\right]\sin\theta\,. \tag{S33d}$$

While a detailed analysis of fixed points and their stability is more challenging in this case and is left for future work, the structure of the amplitude and phase equations is clearly very similar to the one discussed in the main text. In particular, a traveling modulation will again correspond to a solutions with $\sin\theta \neq 0$ and

$$\left[(\kappa - \delta)\rho_A^{-1}\rho_B + (\kappa + \delta)\rho_A\rho_B^{-1}\right] = 0\,, \tag{S34}$$

$$\left[(\kappa - \delta)\rho_A^{-1}\rho_B - (\kappa + \delta)\rho_A\rho_B^{-1}\right] \neq 0 \tag{S35}$$

to guarantee a finite value of $v = \dot{\Phi}/2$. These conditions immediately give $v = \pm\sqrt{\delta^2 - \delta_c^2}$, which provides an excellent fit to the velocity obtained from simulations, as shown in Fig. S5c.

VI. EXAMPLES ON NONRECIPROCITY IN PHYSICAL SYSTEMS

The generic theory described in the main text suggests that nonreciprocity provides a generic mechanism for a static-to-traveling transition in a field theory of coupled scalar fields that exhibit spatial domains or patterns. In this section we provide two examples of how this generic behavior can emerge from specific microscopic models.

A. Example 1 : microscopic nonreciprocity

Let us consider a mixture of particles where the microscopic interactions between the two species are nonreciprocal. Instances of this include mixtures of chemically interacting colloids that are known to exhibit nonreciprocal effective interactions [7, 8] and chase-and-run dynamics in predator-prey systems [9, 10]. Let us assume that such nonreciprocal interactions can be captured by pairwise additive short ranged central forces. Under such circumstances, the microdynamics of the particles' positions $\{\mathbf{r}_i^\mu\}_{i=1}^{N_\mu}$, with $\mu = A, B$, is governed by equations of the form

$$\partial_t \mathbf{r}_i^\mu = \sum_{j=1}^{N_\mu} \mathbf{F}^{\mu\mu}(\mathbf{r}_i^\mu, \mathbf{r}_j^\mu) + \sum_{j=1}^{N_\nu} \mathbf{F}^{\mu\nu}(\mathbf{r}_i^\mu, \mathbf{r}_j^\nu) + \boldsymbol{\eta}_i^\mu. \tag{S36}$$

Here, $\boldsymbol{\eta}_i^{\mu}(t)$ is uncorrelated white noise with zero mean and variance $= \langle \eta_{i\alpha}^{\mu}(t)\eta_{j\beta}^{\nu}(t')\rangle = \sqrt{2D}\,\delta_{ij}\delta_{\mu\nu}\delta_{\alpha\beta}\delta(t-t')$, where α, β denote Carthesian components. $\mathbf{F}^{\mu\mu}(\mathbf{r}_i^{\mu}, \mathbf{r}_j^{\mu})$ and $\mathbf{F}^{\mu\nu}(\mathbf{r}_i^{\mu}, \mathbf{r}_j^{\nu})$ are the intra- and inter-species interactions of the form:

$$\mathbf{F}^{\mu\mu}(\mathbf{r}_i^{\mu}, \mathbf{r}_j^{\mu}) = k_r \Theta\left(\sigma_r, r_{ij}^{\mu\mu}\right) \hat{\mathbf{r}}_{ij}^{\mu\mu} + k_{\mu\mu}\Theta\left(\sigma_{\mu\mu}, r_{ij}^{\mu\mu}\right) \hat{\mathbf{r}}_{ij}^{\mu\mu}, \tag{S37a}$$

$$\mathbf{F}^{\mu\nu}(\mathbf{r}_i^{\mu}, \mathbf{r}_j^{\nu}) = k_r \Theta\left(\sigma_r, r_{ij}^{\mu\nu}\right) \hat{\mathbf{r}}_{ij}^{\mu\nu} + k_{\mu\nu}\Theta\left(\sigma_{\mu\nu}, r_{ij}^{\mu\nu}\right) \hat{\mathbf{r}}_{ij}^{\mu\nu}, \tag{S37b}$$

where $\mathbf{r}_{ij}^{\mu\nu} = \mathbf{r}_i^{\mu} - \mathbf{r}_j^{\nu}$ and $r_{ij}^{\mu\nu} = |\mathbf{r}_{ij}^{\mu\nu}|$. The first terms on the right-hand side of(S37) are excluded-volume forces of strenght $k_r > 0$ and range σ_r. The second terms represent longer-range repulsive or attractive interactions of strength $k_{\mu\mu}$, and $k_{\mu\nu}$ and corresponding range $\sigma_{\mu\mu}$, $\sigma_{\mu\nu}$. All forces are piecewise linear, with $\Theta(\sigma, r_{ij}) = 0$ for $r_{ij} > \sigma$ and $\Theta(\sigma, r_{ij}) = \sigma - r_{ij}$ when $r_{ij} < \sigma$. We assume that particles A are attracted to other A particles ($k_{AA} < 0$), so that species A can self-aggregate and form a dense cluster. This qualitatively mimics the aggregation driven by a negative

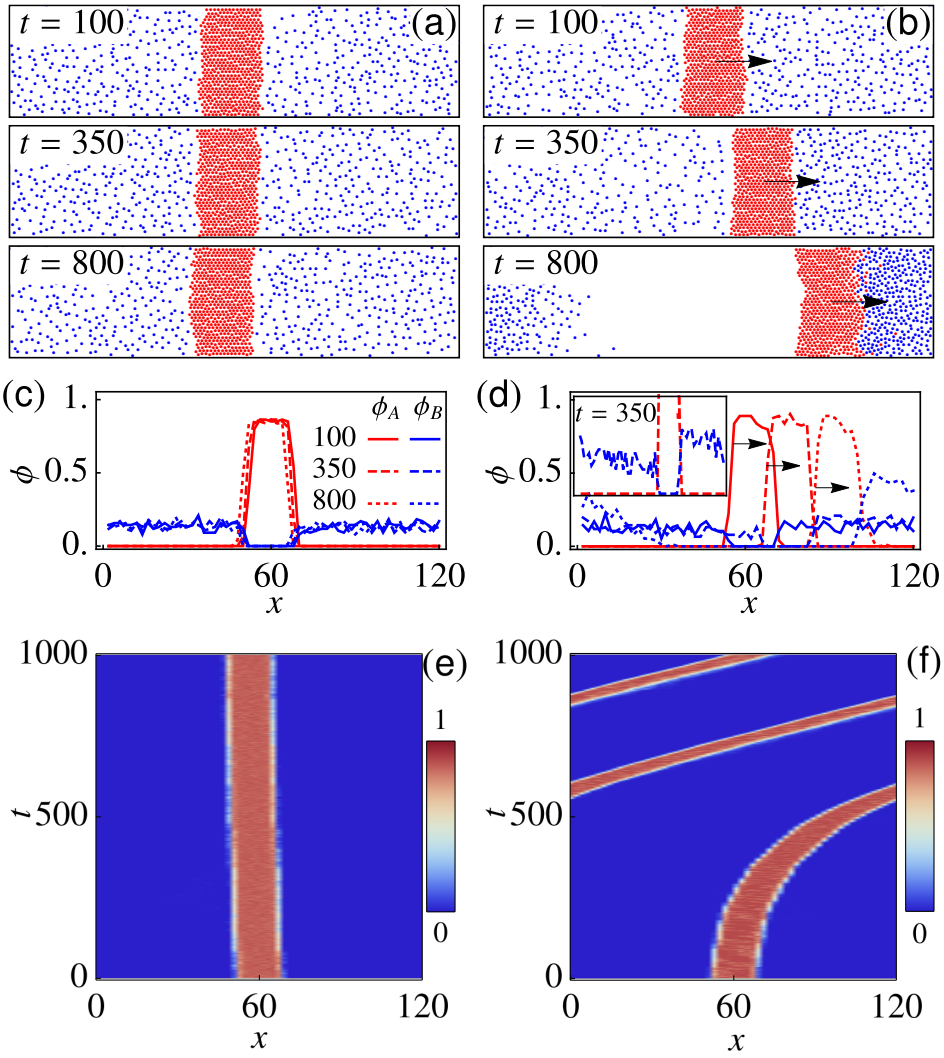

Fig. S6. Transition from static (left panels: a, c, e) to traveling (right panels: b, d, f) states in a binary mixture of attractive-repulsive particles. We use $k_{AB} = -1$ for the left panels, and $k_{AB} = -2$ for the right panels. The red and blue particles represent species A and B, respectively. (a,b) Snapshots of particles at different time points. See also Movies S4-S5 for animation. (c,d) Distributions of particle densities in x at the (c) static and (d) traveling states. The inset in (d) highlights the breaking of reflection symmetry of the blue line. The three different types of lines corresponds to the above three snapshots: solid–$t = 100$, dashed–$t = 350$, and dotted–$t = 800$. We use red and blue lines to indicate densities of species A and B, respectively. (e–f) Spatiotemporal patterns of $\phi_A(x)$ at the (e) static and (f) traveling states. In (c–f), each data point is obtained by measuring the density in a rectangle of width $\Delta x = 2$, spanning the entire vertical direction, and centered at x, i.e. $\phi_\mu(x) = N_\mu(x)/(\Delta x L_y)$, where N_μ is the number of μ particles whose x-positions are within $(x - \Delta x/2, x + \Delta x/2]$.

χ_A in the model B discussed in the main text. To enforce nonreciprocity, we set $k_{AB} < 0$ and $k_{BA} > 0$, so species A (B) is attracted (repelled) by species B (A). As a proof of concept, we have simulated a mixture of $N_A = N_B = 525$ particles in a periodic box of dimension 120×30. The simulation parameters are: $\sigma_r = 1$, $\sigma_{AB} = \sigma_{BA} = 3$, $k_r = 2000$, $D = 1$, $k_{AA} = -2$, $k_{BA} = k_{BB} = 1$, and vary k_{AB} to study the pattern formation. Representative examples shown in Fig. (S6) and Movies S4-S5 indicate that this microscopic model does indeed exhibit the phenomenology discussed in the main body of the paper.

In order to sketch the connection between this microscopic model and the generic theory considered in the main text, let us neglect the noise term in Eq. (S36) and consider the deterministic overdamped microdynamics. The low density dynamics of the density fields $\phi_\mu(\mathbf{r},t) = \sum_{i=1}^{N_\mu} \delta(\mathbf{r} - \mathbf{r}_i^\mu(t))$, will generically be of the form

$$\partial_t \phi_\mu(\mathbf{r},t) = -\boldsymbol{\nabla}_r \cdot [\langle \mathbf{F}_\mu(\mathbf{r},t)\rangle \phi_\mu(\mathbf{r},t)]$$

where $\langle \mathbf{F}\rangle$ is the mean field force, which can be estimated as

$$\begin{aligned}\langle \mathbf{F}_\mu\rangle = &\int d\mathbf{r}' \left(k_r \Theta(\sigma_r, |\mathbf{r}-\mathbf{r}'|) + k_{\mu\mu}\Theta(\sigma_{\mu\mu}, |\mathbf{r}-\mathbf{r}'|)\right) \frac{\mathbf{r}-\mathbf{r}'}{|\mathbf{r}-\mathbf{r}'|}\phi_\mu(\mathbf{r}',t) \\ &+ \int d\mathbf{r}' \left(k_r \Theta(\sigma_r, |\mathbf{r}-\mathbf{r}'|) + k_{\mu\nu}\Theta(\sigma_{\mu\nu}, |\mathbf{r}-\mathbf{r}'|)\right) \frac{\mathbf{r}-\mathbf{r}'}{|\mathbf{r}-\mathbf{r}'|}\phi_\nu(\mathbf{r}',t)\end{aligned}$$

Using the piecewise linear form of the forces, to lowest order in gradients of the density, the mean field force can be evaluated to give

$$\langle \mathbf{F}\rangle = -R_{\mu\mu}\boldsymbol{\nabla}\phi_\mu(\mathbf{r},t) - R_{\mu\nu}\boldsymbol{\nabla}\phi_\nu(\mathbf{r},t)$$

where

$$R_{\mu\nu} = \left(k_r\sigma_r^4 + k_{\mu\nu}\sigma_{\mu\nu}^4\right)\frac{\pi}{6}$$

Therefore, the equations of motion for the macrodynamics of this system are

$$\partial_t \phi_\mu(\mathbf{r},t) = \boldsymbol{\nabla}\cdot[R_{\mu\mu}\phi_\mu(\mathbf{r},t)\boldsymbol{\nabla}\phi_\mu(\mathbf{r},t)] + \boldsymbol{\nabla}\cdot[R_{\mu\nu}\phi_\mu(\mathbf{r},t)\boldsymbol{\nabla}\phi_\nu(\mathbf{r},t)]$$

Focussing on the cross diffusion coefficient, note that in this model, the analog of the reciprocal part of the cross diffusion coefficient is $\kappa_{\mu\nu} = k_r\sigma_r^4\frac{\pi}{6}\phi_\mu$, set by the pairwise repulsive interactions and the analog of the nonreciprocal part is $\delta_{\mu\nu} = k_{\mu\nu}\sigma_{\mu\nu}^4\frac{\pi}{6}\phi_\mu$ and scales with the microscopic nonreciprocal interaction strength. Thus, this microscopic model yields a continuum theory that is closely analogous to the generic theory we considered in the main text and, as shown in Fig. (S6), exhibits the static to traveling pattern transition that is our central result.

B. Example 2 - Emergent nonreciprocity in mixtures of active and passive particles

As a second illustration of a microscopic model giving rise to the phenomenology discussed in this work, we consider a mixture of active (A) and passive (P) Brownian particles [11, 12].

In the absence of interactions, the dynamics of each each Active Brownian Particle (ABP) is described by

$$\partial_t \mathbf{r} = v_0\hat{\mathbf{u}} \tag{S38}$$

where v_0 is the propulsion speed, $\hat{\mathbf{u}} = \cos\theta\hat{x} + \sin\theta\hat{y}$ is the direction of active motion which itself undergoes rotational diffusion, i.e., $\partial_t\theta = \sqrt{2D_R}\xi(t)$ with $\xi(t)$ is a delta-function correlated white noise of unit variance. The ballistic motion exhibited at short times by Eq. (S38) becomes diffusive at long times due to the rotational diffusion of the propulsion direction $\hat{\mathbf{u}}$ with a characteristic diffusion coefficient $v_0^2/2D_R$. In the presense of short range repulsive interactions given by some pairwise additive central potential U_{AA}, a collection of ABPs undergoes a well-studied athermal liquid-gas like phase separation into a dense phase and a low density phase that has been dubbed MIPS (motility induced phase separation) [13]. While the inherently nonequilibrium nature of this phase transition manifests itself in different interfacial phenomena [14, 15], the bulk phenomenology nevertheless is approximately characterized by a supercritical Model B [16, 17].

The second component of our mixture consists of passive Brownian particles that exhibit diffusive dynamics and interact with each other through a short range repulsive potential U_{PP}. This component by itself will form a Brownian gas and its dynamics can be reasonably modeled by a subcritical Model B dynamics [18, 19]. We additionally assume that the two species are coupled through short range repulsive interactions given by a central potential of the form

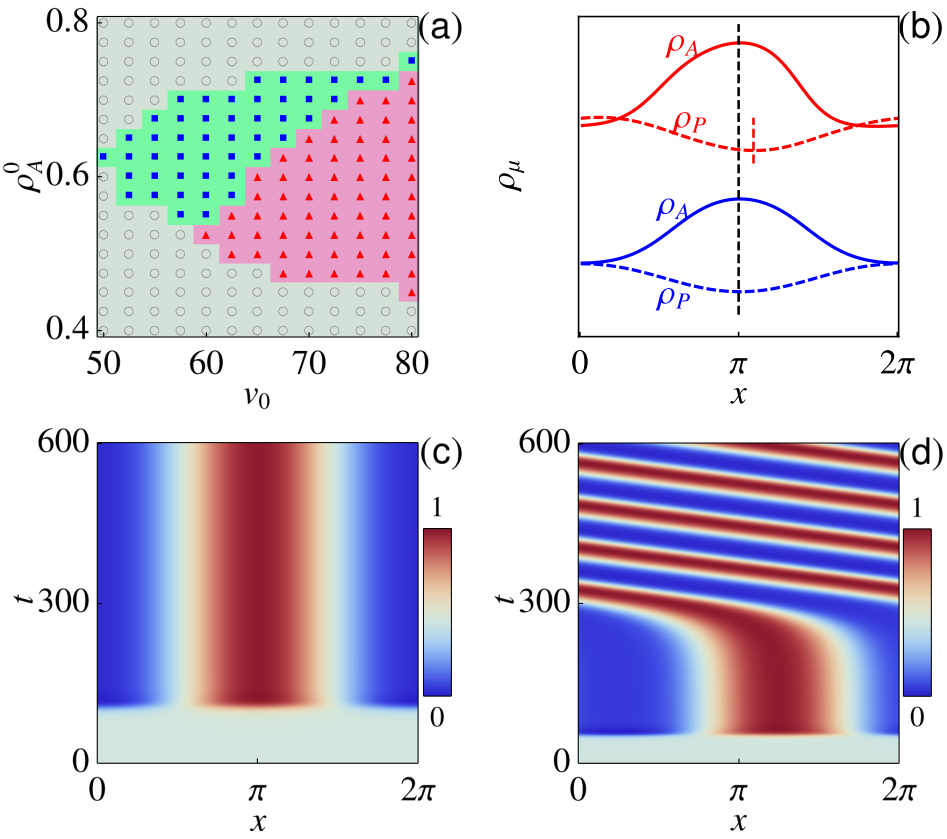

Fig. S7. (a) State diagram of the active-passive mixture spanned by v_0 and ρ_A^0 obtained from numerical simulations of Eq. (S39). As in the model presented in the main text, the AP mixture exhibits three states: a homogeneous state where active and passive particles are mixed (gray, circles), static state where active passive particles are concentrated in different spatial regions, hence demixed (cyan, rectangles), and a state of demixed traveling domains (pink, triangles). (b) Examples of spatial variations of $\rho_A(x)$ (solid lines) and $\rho_P(x)$ (dashed lines) in the static (blue) and traveling states (red). (c–d) Spatiotemporal patterns of $\rho_A(x,t)$ in the (c) static and (d) traveling states. In (b–d), we have used $\rho_A^0 = 0.6$ and (c) $v_0 = 60$ and (d) $v_0 = 70$.

U_{AP}. Precisely such a model was studied through Brownian dynamics simulation in [11] and it was shown that the active and passive particles phase separate and in certain regions of parameter space, the interface between the two species spontaneously starts to move. We demonstrate below that this phenomenon falls within the generic paradigm described in this work.

We stress that at the microscopic level, all interactions in the AP mixture are reciprocal. The corresponding coarse-grained equations as derived in [12] are given by

$$\frac{\partial \rho_A}{\partial t} = \nabla \cdot [D_{AA}\nabla\rho_A + D_{AP}\nabla\rho_P] - \kappa\nabla^4\rho_A \,, \tag{S39a}$$

$$\frac{\partial \rho_P}{\partial t} = \nabla \cdot [D_{PA}\nabla\rho_A + D_{PP}\nabla\rho_P] - \kappa\nabla^4\rho_P \,, \tag{S39b}$$

with diffusion coefficients

$$D_{AA} = a_1^{AA}\rho_A + \frac{v}{2D_R}\left(v - a_0^{AA}v_0\rho_A\right) \tag{S40a}$$

$$D_{AP} = a_1^{AP}\rho_A - \frac{v}{2D_R}a_0^{AP}v_0\rho_A \tag{S40b}$$

$$D_{PA} = a_1^{PA}\rho_P, \tag{S40c}$$

$$D_{PP} = a_1^{PP}\rho_P \,, \tag{S40d}$$

Here, $v = v_0(1 - a_0^{AA}\rho_A - a_0^{AP}\rho_P)$ is the effective motility of active particles and $a_i^{\mu\nu}$ coefficients depend on the pair potentials $U_{\mu\nu}$ and the statistics of interparticle collisions. While there are subtle difference in the form of the direct

diffusion coefficients of this model as compared to our generic Model B, note that the direct diffusion coefficient of species A can be written in the form $D_{AA} \sim \frac{v^2(\rho_A,\rho_P)}{2D_R}$, where $v(\rho_A,\rho_P) = v_0(1 - a_0^{AA}\rho_A - a_0^{AP}\rho_P)$ is the effective density dependent motility of the active particles that are slowed down by collisions with both themselves and with the passive particles. Therefore MIPS driven here by the change in sign of D_{AA} corresponds to the Hopf-bifurcation discussed in our generic theory and can be controlled by the density of either species. Importantly, the cross diffusion coefficients calculated by [12] are indeed nonreciprocal. This nonreciprocity is emergent, in that it arises due to the statistics of the collisions rather than from nonreciprocity of interparticle interactions [12, 20]. The strength of nonreciprocity is controlled by v_0. Even though changing this parameter influences both the direct and cross diffusivities, v_0 can be considered analogue to δ in the generic model considered in the main text. Further, the Hopf bifurcation that controls MIPS rendering the field ρ_A supercritical is now controlled by both the mean densities ρ_A^0 and ρ_P^0. We have studied numerically Eqs. (S39) using $D_R = 3$, $a_0^{AA} = 1$, $a_0^{AP} = 0.7$, $a_1^{AA} = a_1^{AP} = a_1^{PA} = a_1^{PP} = 25$, and $\kappa = 1000$. We have fixed $\rho_P^0 = 0.3$ and tuned ρ_A^0 and v_0, which serve respectively as the analog of the control parameter χ_A and δ in the coupled Model B considered in the main text. The phase behavior of this system is shown in Fig. S7 which reproduces the phenomenology discussed in the main body of the paper. Specifically, by increasing the degree of nonreciprocity v_0, one can see a transition from static out-of-phase pattern (blue rectangles in Fig. S7a, blue lines in Fig. S7b, Fig. S7c) to a steady traveling pattern with broken parity (red triangles in Fig. S7a, red lines in Fig. S7b, Fig. S7d).

[1] J. S. Hesthaven, S. Gottlieb, and D. Gottlieb, Spectral Methods for Time-Dependent Problems, Cambridge Monographs on Applied and Computational Mathematics (Cambridge University Press, 2007).
[2] Z. Lin, H. Ramezani, T. Eichelkraut, T. Kottos, H. Cao, and D. N. Christodoulides, Physical Review Letters **106**, 213901 (2011).
[3] R. El-Ganainy, K. G. Makris, M. Khajavikhan, Z. H. Musslimani, S. Rotter, and D. N. Christodoulides, Nature Physics **14**, 11 (2018).
[4] R. Hanai and P. B. Littlewood, (2019), arXiv:1908.03243.
[5] M. Fruchart, R. Hanai, P. B. Littlewood, and V. Vitelli, (2020), arXiv:2003.13176.
[6] T. Kato, Perturbation Theory for Linear Operators, Classics in Mathematics (Springer Berlin Heidelberg, 1966).
[7] J. Agudo-Canalejo and R. Golestanian, Physical Review Letters **123**, 018101 (2019).
[8] S. Saha, S. Ramaswamy, and R. Golestanian, New Journal of Physics **21**, 063006 (2019).
[9] A. Mogilner, L. Bent, A. Spiros, and L. Edelstein-Keshet, Journal of Mathematical Biology **47**, 353 (2003).
[10] Y. Chen and T. Kolokolnikov, Journal of The Royal Society Interface **11**, 20131208 (2014).
[11] A. Wysocki, R. G. Winkler, and G. Gompper, New Journal of Physics **18**, 123030 (2016).
[12] R. Wittkowski, J. Stenhammar, and M. E. Cates, New Journal of Physics **19**, 105003 (2017).
[13] M. E. Cates and J. Tailleur, Annual Review of Condensed Matter Physics **6**, 219 (2015).
[14] R. Wittkowski, A. Tiribocchi, J. Stenhammar, R. J. Allen, D. Marenduzzo, and M. E. Cates, Nature Communications **5**, 4351 (2014).
[15] M. E. Cates, "Active field theories," (2019), arXiv:1904.01330.
[16] J. Stenhammar, A. Tiribocchi, R. J. Allen, D. Marenduzzo, and M. E. Cates, Physical Review Letters **111**, 145702 (2013).
[17] G. S. Redner, C. G. Wagner, A. Baskaran, and M. F. Hagan, Physical Review Letters **117**, 148002 (2016).
[18] M. Kardar, Statistical Physics of Particles (Cambridge University Press, 2007).
[19] M. Doi, Soft Matter Physics (OUP Oxford, 2013).
[20] Z. You, A. Baskaran, and M. C. Marchetti, Unpublished.

Captions to supplemental movies

S1. **Static.mp4.** Development of static state in the two-dimensional system, corresponding to Fig. S4a-S4b. The color indicates local concentration as displayed in the color-bar on the right of each panel. The video is obtained by integrating Eq. (1) in the main text in a periodic square box $L \times L$ with $L = 2\pi$, but ignoring the ϕ_B^2 term in the self-diffusivity of species B. The parameters are the same as those in the main text: $\chi_A = -0.05$, $\chi_B = 0.005$, $\gamma_A = 0.04$, $\gamma_B = 0$, $\kappa = 0.005$. The degree of nonreciprocity $\delta = \kappa$.

S2. **Traveling.mp4.** Development of traveling state in the two-dimensional system, corresponding to Fig. S4c-S4d. The setting is identical to that in Static.mp4, but the degree of nonreciprocity is $\delta = 3\kappa$.

S3. **Oscillatory.mp4.** Development of oscillatory state in the two-dimensional system, corresponding to Fig. S4e-S4f. The high concentration region of each species periodically splits and merges, performing a run-and-chase game in the two-dimensional space. The setting is the same as that in Traveling.mp4, but starts from a different random initial condition.

S4. **Static-AR.mp4.** Static state in the binary mixture of attractive-repulsive particles, corresponding to Fig. S6a. The video is obtained by simulating $525 + 525$ particles with Eqs. (S36)-(S37) in a periodic box of size 120×30. At the beginning of the simulation, we place a dense cluster of red particles (i.e. species A). As the system evolves, the red cluster remains the same lane formation, but the lane as a whole exhibits diffusive dynamics in the horizontal direction. The parameters are: $\sigma_r = 1$, $\sigma_{AB} = \sigma_{BA} = 3$, $k_r = 2000$, $k_{AA} = -2$, $k_{AB} = -1$, $k_{BA} = k_{BB} = 1$.

S5. **Traveling-AR.mp4.** Traveling state in the binary mixture of attractive-repulsive particles, corresponding to Fig. S6b. The setting is the same as that in Static-AR.mp4, but with $k_{AB} = -2$.